Supporting Information for

Approaching Multi-Structured SnS Nanocrystals toward Enhanced Performance for Photovoltaic Devices

Xin Guo, Hao-Jun Xie, Jia-Wei Zheng, Hao Xu, Qian-Kun, Wang, Yan-Qing Li,Shuit-Tong Lee, and Jian-Xin Tang**

Institute of Functional Nano & Soft Materials (FUNSOM), Jiangsu Key Laboratory for Carbon-Based Functional Materials & Devices, and Collaborative Innovation Center of Suzhou Nano Science and Technology, Soochow University, Suzhou 215123 (P. R. China)

Experimental Section:

Materials: $SnCl_2$ (98%), oleic acid (OA, 90%), trioctylphosphine oxide (TOPO, 98%), poly(3-hexylthiophene) (P3HT) and [6,6]-phenyl-C61-butyric acid methyl ester (PCBM) were purchased from Aldrich. Polyvinylpyrrolidone (PVP), thiourea, *N*-acetyl-*L*-cysteine (NAC), triethylamine (TEA), dodecyl mercaptan (DDM), dodecylamine (DDA), toluene, hexane, ethanol and isopropanol were all supplied by Sinopharm Chemical Reagent Co., Ltd (Shanghai, China) and used as purchased without further purification. High-purity water with a resistivity of greater than 18 M·cm was used in the experiments.

Synthesis of Nanocrystals: Typically, 0.5 mmol $SnCl_2$, 0.25g PVP and 1g OA were mixed in 15 mL high-purity water and stirred vigorously for 30 min in nitrogen atmosphere to form the emulsion solution A. Thiourea (1 mmol) was dissolved in 5 mL high-purity water to form solution B. Solution B was then added dropwise into the PVP and OA contained solution A and mixed sufficiently for 1 h to form solution C. Afterwards, 1 mmol ligand (NAC, TEA, DDM, DDA or TOPO) were added into the above solution C and stirred for 3 h to complete the ligand exchange. After that,

the mixture was sealed into a 30 mL Teflon-lined autoclave, heated to 160 ^{o}C and maintained at this temperature for 10 h. After the autoclave was cooled down to room temperature naturally, the NAC, DDM or TEA capped products in aqueous phase were separated and washed with high-purity water and then ethanol three times. The final products were dispersed in water for later use. For the OA, DDA and TOPO capped products in oil phase, a hexane/isopropanol mixture (1:1) was added to the crude solution and the nanocrystals were isolated by centrifuging. The products were additionally purified twice by re-dispersing them in hexane and precipitating with isopropanol. Finally, the purified nanocrystals were dispersed in common organic solvents such as toluene for later use.

Device Construction: The PV devices were constructed by using NAC-capped SnS NWMs as hole transporting layer (HTL). The indium tin oxide (ITO)-coated glass substrates with a sheet resistance of 20 Ω per sq. were cleaned in sequence by Decon 90, deionized water, ethanol under ultrasonication for 20 min, respectively, and then dried in an oven. The HTL was prepared by spin coating the bare SnS NWMs solution on the UV-ozone treated ITO glass substrates, and then thermally annealing at 140 ^{o}C for 15 min in air. The prepared ITO glass substrates with SnS NWMs were then transferred into a nitrogen-filled glove box for spin-coating the blend of poly(3-hexylthiophene):[6,6]-phenyl-C61-butyric acid methyl ester (P3HT:PCBM) with a 1 : 0.8 weight ratio (10 mg·mL^{-1}, dissolved in dichlorobenzene) on top of the buffer layer at 600 rpm for 2 min. The wet film was subjected to solvent annealing and a thermal annealing at 110 ^{o}C for 10 min. Finally, the LiF(0.5 nm)/Al(100 nm) bilayer cathode was deposited by thermal evaporation in a high vacuum system at a base pressure of 2×10^{-6} Torr. The deposition rate and film thickness were monitored by a quartz crystal oscillator. A shadow mask was used to define the Al cathode, and the device area determined by the overlap between ITO anode and metal cathode was estimated to be 0.1 cm^2. For comparison, PVCs with and without the pristine SnS NWMs as HTL were fabricated with identical process parameters during the same batch processing.

Characterization:

Transmission electron microscopy (TEM): The particle diameter, lattice fringes, the electron diffraction pattern and the EDX spectra were obtained by using a FEI Tecnai G2 F20 transmission electron microscope. A drop of corresponding carbon dot aqueous solution was placed on a copper grid that was left to dry before transferring into the TEM sample chamber. The particle diameter was estimated by using ImageJ software analysis of the TEM micrographs.

Spectroscopy: The crystal structure was analyzed by PANalytical Empyream multi-functional X-ray diffractometer (XRD). The UV–*vis* absorption of the sample was recorded at room temperature with a Perkin Elmer Lambda 750 UV/Vis/NIR spectrophotometer. Photoluminescence (PL) spectra were recorded on a Hitachi F-4600 fluorescence spectrophotometer. For the device construction, the thickness of each layer was measured using the alpha-SE TM Spectroscopic Ellipsometer (J. A. Woollam Co., Inc). The electronic structures of the samples were determined by X-ray photoelectron spectroscopies (XPS) in a Kratos AXIS Ultra-DLD ultrahigh vacuum system (a base pressure of 3×10^{-10} Torr) with monochromatic Al Kα source (1486.6 eV for XPS). UPS analysis was performed to characterize and the vacuum level (VL) and highest occupied molecular orbital (HOMO) with an unfiltered He I (21.2 eV) gas discharge lamp and a total instrumental energy resolution of 100 meV.

Quantum yield calculation: Quantum yield (QY) was measured according to established procedure (Lakowicz, J. R. Principles of Fluorescence Spectroscopy, 2nd Ed., 1999, Kluwer Academic/Plenum Publishers, New York) by using quinine sulfate in 0.10 M H_2SO_4 solution as the standard (Φ=0.54). The quantum yield was calculated using the following equation:

$$Q = Q_R \frac{I}{I_R} \frac{A_R}{A} \frac{n^2}{n^2{}_R}$$

Where Q is the quantum yield, I is the measured integrated emission intensity, A is the optical density and n is the refractive index (taken here as the refractive index of

the respective solvents). The subscript R refers to the reference fluorophore of known quantum yield.

The UV-*vis* absorption spectrometer was used to determine the absorbance of the samples. The concentration of the samples for QY estimation should allow the first excitonic absorption peak to be below 0.05 in order to avoid any significant reabsorption. A spectrophotometer with an excitation slit width of 0.25 and an emission slit width of 0.25 was used to excite the samples and to record their photoluminescence spectra.

Device characterization: The current density–voltage (*J-V*) characteristics of the PVCs without any encapsulation were examined in air at room temperature using a programmable Keithley 2612 source measure unit under illumination from a 150 W Newport 91160 solar simulator with an air mass (AM) 1.5 G filter. The illumination intensity was adjusted to be 100 $mW \cdot cm^2$, which was calibrated using a standard Si optical power meter. The incident photon to current conversion efficiency (IPCE) measurement was conducted with a photo-modulation spectroscopic setup (Newport monochromator).

Results:

Table S1. The information of the number of particle counted (*n*), the mean particle diameter (*D*), and the standard deviation (SD) for the resulted SnS nanocrystals derived from TEM images shown in Figure 1 by self-developed digital statistic software.

Ligand	Control	TOPO	DDM	NAC (length)
n	35	29	37	27
D (nm)	3.66	5.14	9.15	8.78
SD (nm)	0.36	0.73	1.01	1.30

From the TEM images, we can see that the particles have excellent dispersibility, which may benefit from the existence of polyvinylpyrrolidone (PVP) as stabilizer.

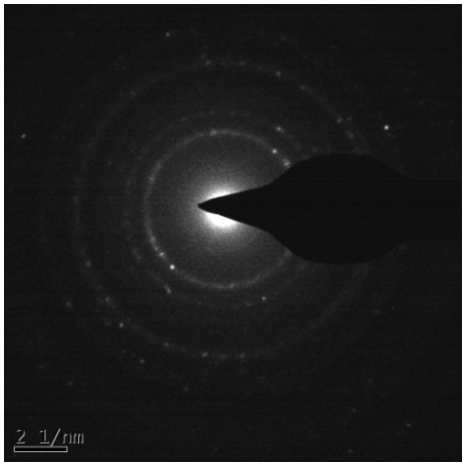

Figure S1. The electron diffraction pattern of the as-prepared control SnS samples.

Table S2. The crystal characteristics of the resulted nanocrystals derived from the PXRD patterns shown in Figure 2B: the standard data of JCPDS No which are well matched, crystal system and the space group.

Ligand	Ref. JCPDS No.	Crystal system	Space group
Control	75-0925	Orthorhombic	pmcn
TOPO	33-1375	Orthorhombic	pbnm
DDM	39-0354	Orthorhombic	pbnm
NAC	75-1803	Orthorhombic	pbnm
DDA	14-0620	Orthorhombic	pbnm
TEA	06-0359 (SnO)	Tetragonal	P4/nmm
	73-1859 (SnS)	Orthorhombic	pnma

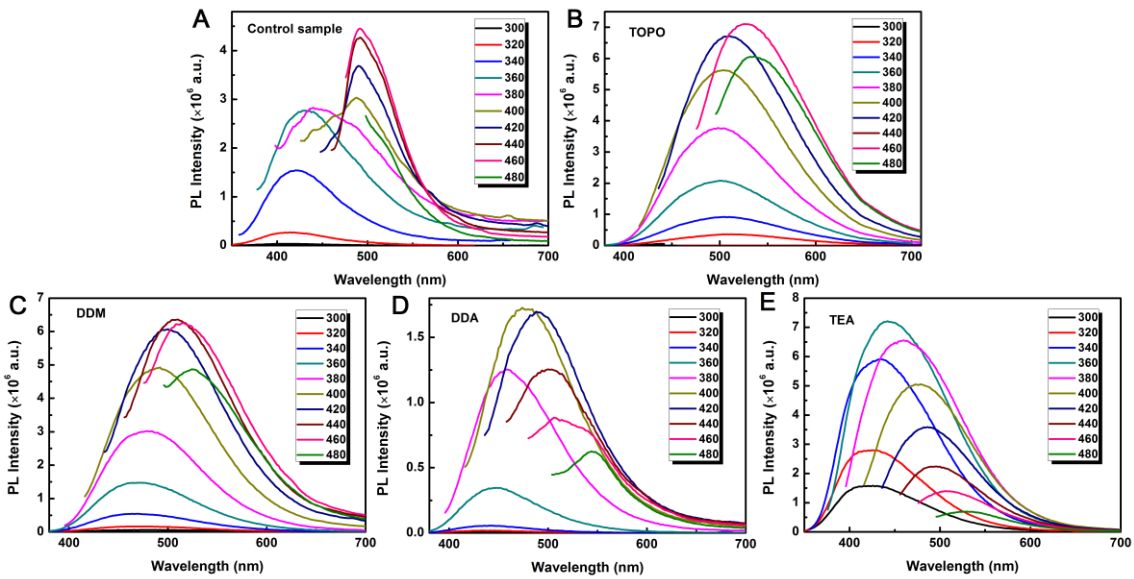

Figure S2. PL spectra of the resulted SnS or SnO/SnS nanocrystals at different excitation wavelength (in 20 nm increment stating from 300 nm to 480 nm).

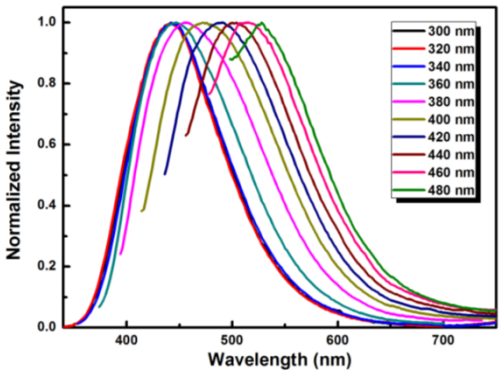

Figure S3. Normalized PL spectra of SnS NWMs at different excitation wavelength (in 20 nm increment stating from 300 nm to 480 nm).

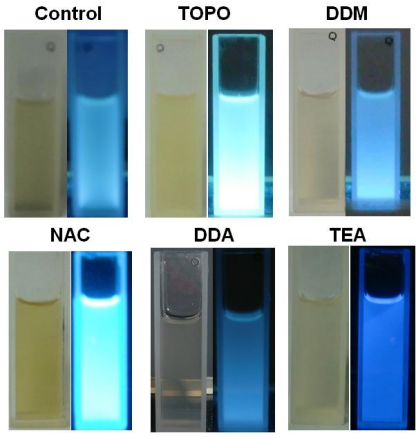

Figure S4. The corresponding photographs of SnS nanocrystal solution with different ligands under daylight and UV lamp (λ_{ex} = 365 nm).

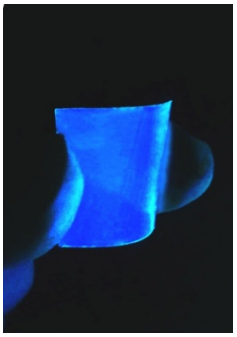

Figure S5. The photograph of the blue-light-emitting flexible plastic sheet coated with TEA-functionalized SnO/SnS nanobelt solution under UV illumination (λ_{ex} = 365 nm).

Table S3. The quantum yield (QY) of the corresponding SnS or SnO/SnS products with different ligands.

Ligand	Control	TOPO	DDM	NAC	DDA	TEA
QY (%)	2.40	5.17	5.20	5.82	1.30	6.86

With the quinine sulfate in 0.10 M H_2SO_4 solution as the standard (Φ=0.54), the quantum yield (QY) of the resulted samples were determined. As shown in Tab. S3, the QYs of the samples vary apparently, from which we can see the TEA – functionalized SnO/SnS nanobelts have the highest QY (6.86%), while the DDA-capped SnS nanowires behaves weak fluorescence (QY=1.30%).

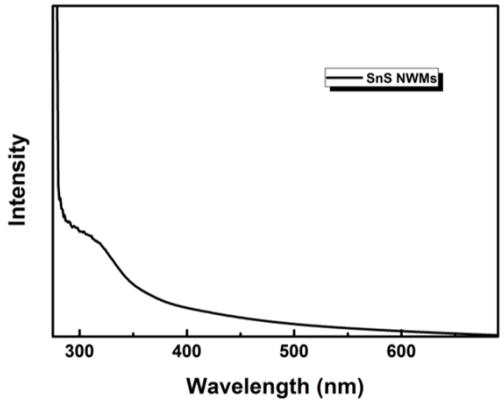

Figure S6. UV-*vis* absorption spectra of the NAC-functionalized SnS NWMs.

The direct band gap of the SnS NWMs with about 2.9 eV was estimated from the UV-*vis* absorption spectra, which is similar to previous report.[1]

References

[1] J. Ning, K. Men, G. Xiao, L. Wang, Q. Dai, B. Zou, B. Liu, G. Zou, *Nanoscale* **2010**, *2*, 1699-1703.